Muon doses at earth surface
above the Linear Collider:
Improved calculations

G. Baur, A. Leuschner, K. Tesch

"Die Verantwortung für den Inhalt dieses
Internen Berichtes liegt ausschließlich beim Verfasser"

Muon doses at earth surface
above the Linear Collider:
Improved calculations

G. Baur[‡‡], A. Leuschner, K. Tesch

Abstract

At the proposed Linear Collider an electron and a positron beam of 250 GeV energy and 8 MW beam power each have to be absorbed about 10 m under ground. In order to estimate the muon dose at earth surface pair production cross sections are nessesary for large angles. They are calculated for incoherent muon photoproduction processes from nucleons in the region up to $100\,\mathrm{GeV}^2$ momentum transfer in addition to the coherent production from a nucleus. The recieved expressions are parametrized for use in numerical dose calculations. The maximum annual doses are about $50\,\mu\mathrm{Sv}$, 20 times less than the natural radiation dose.

[‡‡]Forschungszentrum Jülich, Institut für Kernphysik, D-52425 Jülich

1 Introduction

Muon doses at earth surface above a proposed $e^+ - e^-$ Linear Collider $(2 \cdot 250$ GeV) were estimated in a previous report [1]. The sources of muons are the absorbers into which the beams are dumped after having passed the interaction region, and the distributed collimator systems. Relevant muon production angles are as high as 200 mrad, and this is an unusual kinematical region in this context. Therefore not all cross-sections for the contributing pair production processes were available. Analytical expressions for the double-differential cross-sections for the coherent muon production from a nucleus with and without form factor were used, whereas only some numerical data [4] were available for the elastic and inelastic production from a nucleon. As the result, only upper and lower limits of muon doses could be given differing by about 4 orders of magnitude. It was not possible to pin down muon doses more accurately though qualitative arguments were derived that they will be lower than the natural radiation background.

The use of cross-sections for coherent production without form factors corresponding to a very heavy point-like nucleus is an allowed approximation only for very small angles, at large angles it gives a huge overestimation. A nucleus with form factor is considered as an extended charge distribution, muon production from this field dominates all other production mechanisms in forward direction. But the larger the scattering angle the higher the momentum transfer and the smaller the object that really scatters. The momentum transfer from the muon to the nucleus $q \approx \theta E$ (see section 3) can be translated by means of the Heisenberg uncertainty relation to the dimension of the scattering object $r \approx \hbar c/(\theta E)$. A typical muon energy of 120 GeV and angle of 0.08 rad lead to momentum transfers up to $q^2 = 100\,\text{GeV}^2$ and to dimensions down to 0.02 fm, 100 times smaller than a carbon nucleus (3 fm). That is the reason why the cross-section at large angles is dominated by elastic and inelastic processes from a single nucleon and not from an entire nucleus.

In the present paper first we describe the method of muon dose calculation in greater detail, see also [2]. In section 3 we describe the approximations used to calculate all relevant photoproduction processes, coherent and incoherent ones. Section 4 presents our quantitative results on muon doses.

In our previous report [1] the contributions of muons from pion and kaon decay were simulated with the Monte Carlo Code FLUKA. In fact, no muon was found with the nessesary range to penetrate the soil above the tunnel. Therefore the contribution of these processes is much smaller than that from the photoproduction processes.

2 The muon dose calculation

Muon fluence from the electro-magnetic cascade (EMC). The differential muon fluence $d^2\Phi/(d\Omega\, dE)$ from the EMC initiated by one electron is the result of the integration of the cross-section (see section 3) and the photon track length over all photon energies:

$$\frac{d^2\Phi}{d\Omega\, dE}(E,\theta) = \frac{2}{R^2} \int_{E+m_\mu}^{E_o-m_e} \frac{d^2\sigma}{d\Omega\, dE}(k,E,\theta) \cdot \frac{dl}{dk}(k)\ dk \quad \text{in} \quad \left(\frac{1}{\text{cm}^2\,\text{GeV}\,\text{sr}}\right) \qquad (1)$$

The symbols are:

θ	production angle in the laboratory frame,
R	distance to the target,
X_o	radiation length,
E_o	total energy of the primary Electrons,
E	total muon energy,
k	energy of the photon in the EMC,
m_e	rest mass of the electron,
m_μ	rest mass of the electron,
$d^2\sigma/(d\Omega\, dE)$	energy-angle-distribution of the muons in $1/(X_o\,\text{GeV}\,\text{sr})$,
dl/dk	differential photon track length in the EMC in (X_o/GeV).

The modell of CLEMENT and KESSLER is used for the differential photon track length in the EMC:

$$\frac{dl}{dk} = \frac{1}{k} \cdot \frac{0.964\,(k/E_o)}{0.686\,(k/E_o)^2 - 0.5\,(k/E_o)^4 - ln\,[1-(k/E_o)^2]} \qquad (2)$$

Muon transport. In a second step the differential muon fluence is convoluted with a scattering angle distribution taking multiple scattering into account when travelling through thick materials (see fig.1):

$$\frac{d\Phi}{dE}(E,\theta') = \int_0^{\theta_{cut}} \frac{d^2\Phi}{d\Omega\, dE}(E,\theta) \cdot I_o\left(\frac{\theta \cdot \theta'}{\theta_c^2(E)}\right) \cdot e^{-\frac{1}{2}(\theta^2+\theta'^2)/\theta_c^2(E)}\, \theta\, d\theta \qquad (3)$$

where:

θ'	angle of the scattered muon in the lab frame,
θ_{cut}	upper integration limit[1] ($0.5\,rad = 28.6°$),
$I_o(x)$	Besselfunction of the first kind.
$\theta_c^2(E) = 2A_2(E)/R^2$	square of the characteristic angle of the angle distribution, where
$A_2(E)$	mean square of the lateral displacement obtained by an additional integration (see [2])

The square of the characteristic angle θ_c^2 is calculated by the theory of EYGES [2] where the production angle as well as the scattering angle are considered as small. In our previous report we compared the shielding experiments with 240 GeV and 280 GeV muons at CERN with our

---

[1] The integration is usually done in the range $0\ldots\pi$. Since the integrand of (3) steeply falls for $\theta > \theta'$ the integration is stopped at $\theta_{cut} = \theta' + 3\sqrt{\theta_c^2}$. As it is an approximation for small angles, θ' should be less than 0.45 rad.

calculations and found that the calculated θ_c^2 are about 3 times smaller than the experimental ones at those muon energies. Thus, we multiply all θ_c^2 by a factor of 3 for our dose calculations.
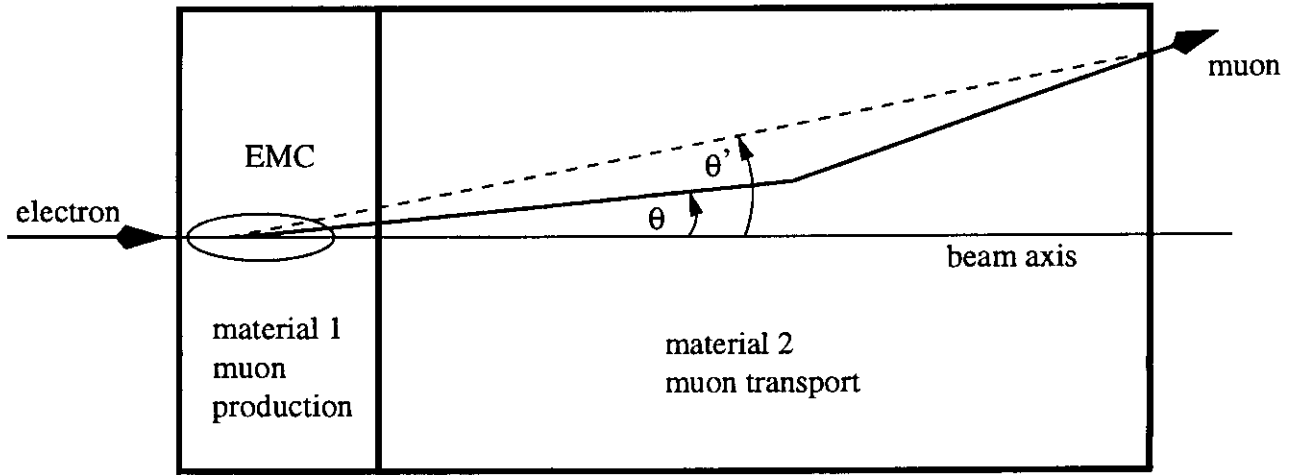
Figure 1: Sketch of the geometry used for muon transport.

In the last step the muon fluence is integrated over all muon energies and multiplied by the fluence-to-dose conversion factor $h_\mu = 3.5 \cdot 10^{-10}$ Sv cm^2.

$$D(\theta') = h_\mu \cdot \int_{E_R}^{E_o - m_e} \frac{d\Phi}{dE}(E, \theta') \, dE \qquad (4)$$

The absorption of muons is taken into account by the lower integration limit E_R. It is the energy that muons loose by penetrating both materials.

3

3 Cross-sections for photoproduction of muon pairs (Bethe-Heitler process)

The cross-section for the QED process $\gamma + Z \to l^+ l^- + X$ with $(l = e, \mu)$ is in principle well known (Bethe-Heitler formula). Due to the larger mass of the muon as compared to the electron and due to the importance of larger scattering angles for the present problem the structure of the nucleus Z is important. The necessary information is contained in the form factors. They are known in the kinematical region under discussion and simple parametrizations exist, which are satisfactory for the present purpose.

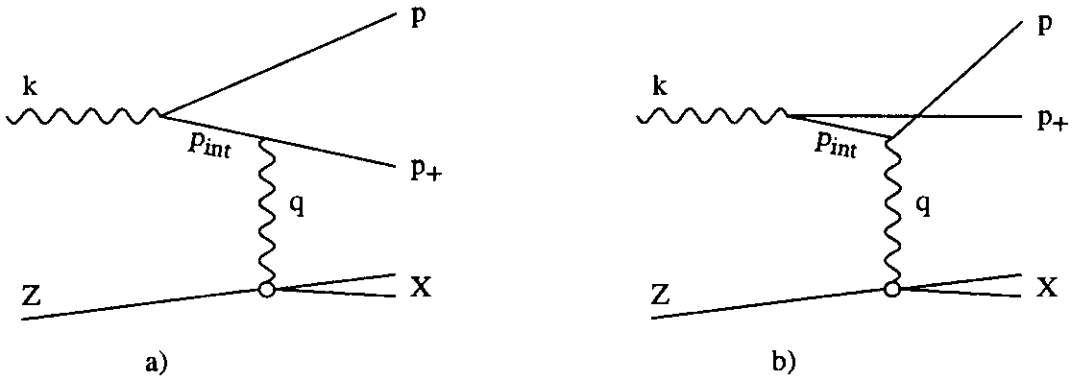The process is described by two graphs [2] given schematically as

Figure 2: Feynman graphs describing the process $\gamma + Z \to p + p_+ + X$

We are interested in the case where only one muon (say μ^- with momentum p) is observed and the momentum p_+ is integrated. The most complete calculation of this problem seems to be given by Y. S. Tsai [4] (eq.2.3). An exact formula is given there, which is quite difficult to handle in the general case.

We use two approximations to work out all the relevant contributions. The Weizsäcker-Williams approximation, which is also used in [4, 5], assumes a very small q^2 of the exchanged photon. The square of the four-momentum transfer q^2 is given by $q^2 = q_o^2 - \vec{q}^2$. For real (massless) photons we would have $q_o = |\vec{q}|$, i.e. the Einstein relation $q^2 = 0$ (energy of the photon = momentum of the photon). It allows the calculation of the coherent production from an extended nucleus and two of the incoherent production mechanisms, namely the elastic and the $p - \Delta$ inelastic productions from a nucleon. For the case of a high momentum transfer we take the muon pole approximation (see graph b) to calculate the muon production from a nucleon in the deep inelastic region as it was given in [6] (see also [8]).

In the following subsections we give formulae for the calculation of all production mechanisms. Results are shown in fig.3,4 for one example: photon energy $k = 200 \, \text{GeV}$ und muon energy $E =$

---

[2]apart from higher order effects which can be taken into account using the Bethe-Maximon theory (see equ. 3.3 in [4]). They are dropped here as they are small for small Z and would only decrease the cross-section.

120 GeV. These parameters are typical for our case. A muon energy of 120 GeV corresponds to a range in soil of 238 m which gives a minimum angle θ_R of 0.042 rad with a 10 m thick soil layer above the tunnel. That means: muons with larger angles do contribute to the dose at the earth surface whereas muons with smaller angles do not. Therefore θ_R is the lower limit of the angular region of interest.

3.1 Weizsäcker-Williams approximation

The practical calculations were done in an approximation shown to be generally good [5]. In this approximation, the main contribution comes from the region where q^2 of the exchanged photon is smallest (Weizsäcker-Williams or equivalent photon approximation) close to the pole of the matrix element for $q^2 = 0$ (real photon) (eqs.3.5, 3.6 of [4], see also eq.2.19 of [5]). In order to realize a minimum q^2 the μ_+ and the μ_- scatter to opposite sides with transverse momenta being of about equal magnitude. In this framework, numerical calculations were performed for our relevant energies. Some of the numerical results of Tsai [4] were reproduced as a check of our calculations.

The muon production cross-section has the general form

$$\frac{d^2\sigma}{d\Omega\,dE} = \left(\frac{hc}{2\pi}\right)^2 \cdot \frac{2\alpha^3}{\pi k} \cdot \frac{E^2}{m_\mu^4} \cdot \left[\frac{2x^2 - 2x + 1}{(1+L)^2} + \frac{4x(1-x)L}{(1+L)^4}\right] \cdot \chi \tag{5}$$

where $x = E/k$ and $L = \left(\frac{\theta}{m_\mu/E}\right)^2$. The effects of the electromagnetic structure of the target are contained in the function

$$\chi = \frac{1}{2m_i} \int\limits_{t_{min}}^{t_{max}} \frac{dt}{t^2} \int\limits_{m_i^2} dm_f^2 \left[(t - t_{min}) \cdot W_2 + 2t'_{min} \cdot W_1\right] \tag{6}$$

where $t = -q^2$ the momentum transfer, m_i, m_f the initial and final mass and W_2 and W_1 the form factors mainly representing the distributions of the electric charge and the magnetic dipole respectively. Expressions for the minimal and maximal momentum transfer t_{min} and t_{max} are given in [4], equ.(2.9). The most important contributions to this integral come from the region close to t_{min} ($t_{min} = 0$ corresponds to the photon pole). Due to the kinematics, the value of t_{min} is usually quite low ($t_{min} \leq 1\text{GeV}^2$) except in the angular range which is very close to the kinematical limit. [3].

3.1.1 Coherent production from an extended nucleus.

The main contribution to the cross-section is due to coherent scattering from the nuclei (proportional to Z^2) at very small angles. At larger angles, the effects of the elastic scattering are strongly reduced due to the nuclear form factor. This form factor describes the extended nuclear charge distribution and is well known from elastic electron scattering:

$$W_2^{coh} = 2m_N \; \delta(m_f^2 - m_N^2) \cdot \frac{Z^2}{(1 + t/d)^2} \qquad \text{and} \qquad W_1^{coh} = 0 \tag{7}$$

---

[3]Here ($t_{min} \geq 1\text{GeV}^2$) the Weizsäcker-Williams approximation becomes worse, as is also noted in [5],p.3121.

where m_N is the mass of the nucleus and $d = 0.164/A^{2/3}\mathrm{GeV}^2$ representing the dimension of the nucleus. With these form factors, the integral (6) can be solved analytically. Thus, this cross-section is well suited for dose calculations.

3.1.2 Elastic production from a nucleon.

At the larger q^2 values, the structure of the nucleus is resolved into its constituents, mainly the nucleons (neutrons and protons). We assume now that the nucleus is an assembly of neutrons and protons at rest in the laboratory.

For our purpose the electromagnetic form factors of the nucleons can be well parametrized in its usual dipole form (B.44 of [4]).

$$\begin{bmatrix} W_2^{p,el} \\[1em] W_1^{p,el} \\[1em] W_2^{n,el} \\[1em] W_1^{n,el} \end{bmatrix} = 2m_p\, \delta(m_f^2 - m_p^2)\, \frac{1}{(1 + t/\Lambda^2)^4} \begin{bmatrix} \frac{1 + \mu_p^2\, t/(4m_p^2)}{1 + t/(4m_p^2)} \\[1em] \mu_p^2\, t/(4m_p^2) \\[1em] \frac{\mu_n^2\, t/(4m_p^2)}{1 + t/(4m_p^2)} \\[1em] \mu_n^2\, t/(4m_p^2) \end{bmatrix} \tag{8}$$

where $\mu_p = 2.79$ and $\mu_n = -1.91$ denote the magnetic dipole moments of the proton and the neutron in units of the nuclear magneton respectively and $\Lambda^2 = 0.71\mathrm{GeV}^2$. Eqs.(5),(6) and (8) are taken to calculate the cross-sections for the elastic production from a proton and from a neutron. For the kinematical parameters of our example (see above) they are displayed in fig.3 as dashed lines. As one can see, both curves behave very similarly at large angles where the contributions of the $W_1 s$ dominate and the ratio is just $(\mu_p/\mu_n)^2 \approx 2$.

3.1.3 Inelastic production from a nucleon (excitation of the Δ-resonance).

In order to include also proton (or neutron) inelastic form factor effects, we proceed as follows: At moderate values of $t = -q^2$, the dominant contribution is due to the excitation of the Δ-resonance which decays $\Delta \to p(n) + \pi$. This can already be seen by looking at the total cross-section for $\gamma + p$ [9]. There exist simple and reliable parametrizations of the form factor for the p-Δ transition. Following G. Chanfray et al. [7] we find for the corresponding form factor (for details see [10])

$$W_2^{p\Delta} = 2m_p\, \delta(m_f^2 - m_\Delta^2)\, \frac{\mu^{\star 2}}{9} \left(\frac{m_\Delta + m_p}{2m_p}\right)^4 \frac{t/4m_p^2}{(1 + t/\Lambda^2)^4} \quad \text{and} \quad W_1^{p\Delta} = 0 \tag{9}$$

with $\mu^\star = 9.42$ and where the Δ-resonance is treated as a stable particle. The resulting cross-section is shown in fig.3 (lower solid line). Its behavior at large angles is very similar to the elastic cross-sections as expected from the t-dependencies of the form factors. Scanning the total γp cross-section from low to high energy the Δ-resonance is the first object followed by two other smaller resonances and later a continuum. The influence of those other parts were qualitatively studied by moving m_Δ towards higher energies with the result that the contributions increase
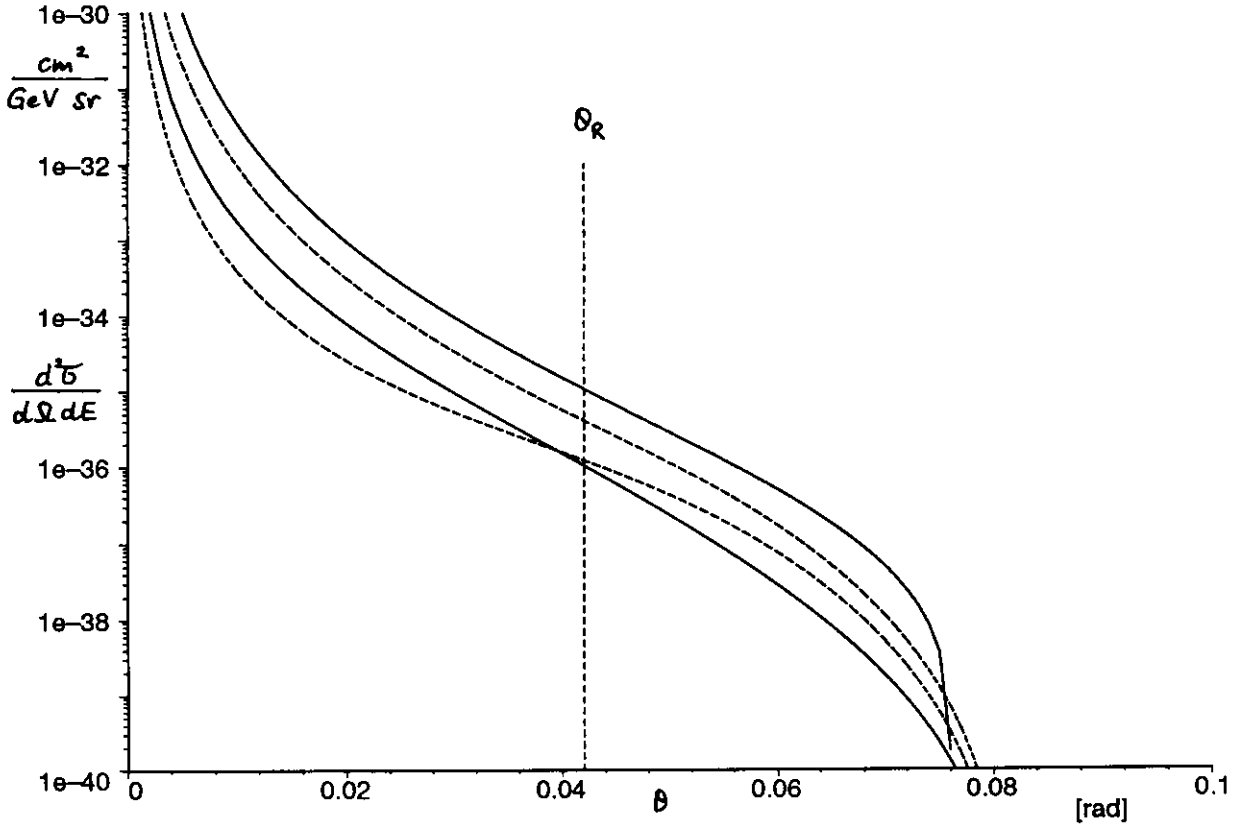
6

Figure 3: Nucleon cross-sections at a photon energy of 200 GeV and a muon energy of 120 GeV. Upper dashed curve: proton elastic, lower dashed curve: neutron elastic. lower solid curve: $p - \Delta$ inelastic, upper solid curve: proton-deep-inelastic.

for small angles but decrease for large angles. As we are mainly interested in large angles the form factor equ.(9) is sufficient for our application. It should be noted here that proton and neutron behave similarly as it is indicated by comparing the γp with the γd cross-section [9].

3.2 Muon pole approximation

In addition to the photon pole contribution there is another important kinematical region which is considered in detail in [6] or [8]. In this case, the scattering angle of the unobserved muon p_+ is very small, see Feynman graph b) in fig.2. After an integration over the unobserved muon p_+ one obtains a simple result: the scattering process transforms into a scattering of a quasi-real muon on the target leading to the general form

$$\frac{d^2\sigma}{d\Omega\,dE} = \left(\frac{hc}{2\pi}\right)^2 \cdot \frac{\alpha^2}{4k^2 \sin^4(\theta/2)} \cdot \left[W_2^\gamma(k,E,\theta)\cos^2(\theta/2) + 2W_1^\gamma(k,E,\theta)\sin^2(\theta/2)\right] \quad (10)$$

with

$$W_{1,2}^{\gamma}(k,E,\theta) = \frac{\alpha}{\pi} \cdot \ln\left(\frac{k}{m_\mu}\right) \cdot \int\limits_{x_o}^{1} dx \left[1 + \left(\frac{1}{x} - 1\right)\right] W_{1,2}(\nu, Q^2) \tag{11}$$

where

$$x_o = \frac{m_p E}{m_p k - 2kE \sin^2(\theta/2)} \quad , \quad \nu = xk - E \quad \text{and} \quad Q^2 = 4xkE \sin^2(\theta/2) \tag{12}$$

3.2.1 Deep inelastic production from a proton.

Using a simple parametrization for the proton structure function (see [10] for details) and neglecting the contributions from W_1 we get

$$W_2^{\gamma}(k,E,\theta) = \frac{\alpha}{\pi} \cdot \ln\left(\frac{k}{m_\mu}\right) \cdot \int\limits_{x_o}^{1} dx \left[1 + \left(\frac{1}{x} - 1\right)\right] \rho \frac{1}{xk - E} \ln\left[\frac{2m_p(xk - E)}{xkE\theta^2}\right] \tag{13}$$

where $\rho = 0.16$ is a parameter. The resulting cross-section is also shown in fig.3 (upper solid curve). It turns out that it dominates all other nucleon cross-sections by at least a factor of 2 at larger angles. For smaller angles the approximation for the structure function used in equ.(13) becomes inaccurate.

3.3 Full cross-section

Now we put together the various cross-sections for dose calculation:

$$\sigma_{(Z,A)} = \sigma_{(Z,A)}^{coh} + \overbrace{Z\sigma_p^{el} + (A - Z)\sigma_n^{el}}^{elastic} + \underbrace{A\sigma_p^{p\Delta} + A\sigma_p^{dis}}_{incoherent} \tag{14}$$

Here the indications of the double differential character were dropped for convenience. The full cross-section (solid curve) and the coherent part (lower dashed curve) are shown in fig.4 for carbon and for our example mentioned above. In the region of interest ($\theta > \theta_R$) the incoherent part is larger by 2 orders of magnitude compared to the coherent one. The dolphin-like shape of the cross-section is due to the kinematical limit for scattering from a nucleon at 0.080 rad, where the incoherent part breaks down to zero for kinematical reasons. The coherent part behaves similarly but at a $\sqrt{12}$ times larger angle: 0.277 rad.

Unfortunately, all the incoherent cross-sections contain integrals that have to be solved numerically. In order to recieve an expression which can be calculated analytically (avoiding a fifth numerical integration in the dose calculation) we replace the whole incoherent part in equ.(14) by

$$\sigma_{(Z,A)}^{incoh} \approx A\sigma^{coh} \quad \text{where} \quad W_2^{coh} = 2m_p \, \delta(m_f^2 - m_p^2) \cdot \frac{1}{(1 + t/d')^2} \quad \text{and} \quad d' = 3 \text{ GeV}^2 \, , \tag{15}$$

compare with equ.(7). The choices $Z = 1$ and $d' = 3\,\text{GeV}^2$ have no physical background but have the purpose to approximate the complete incoherent contribution as closely as possible;
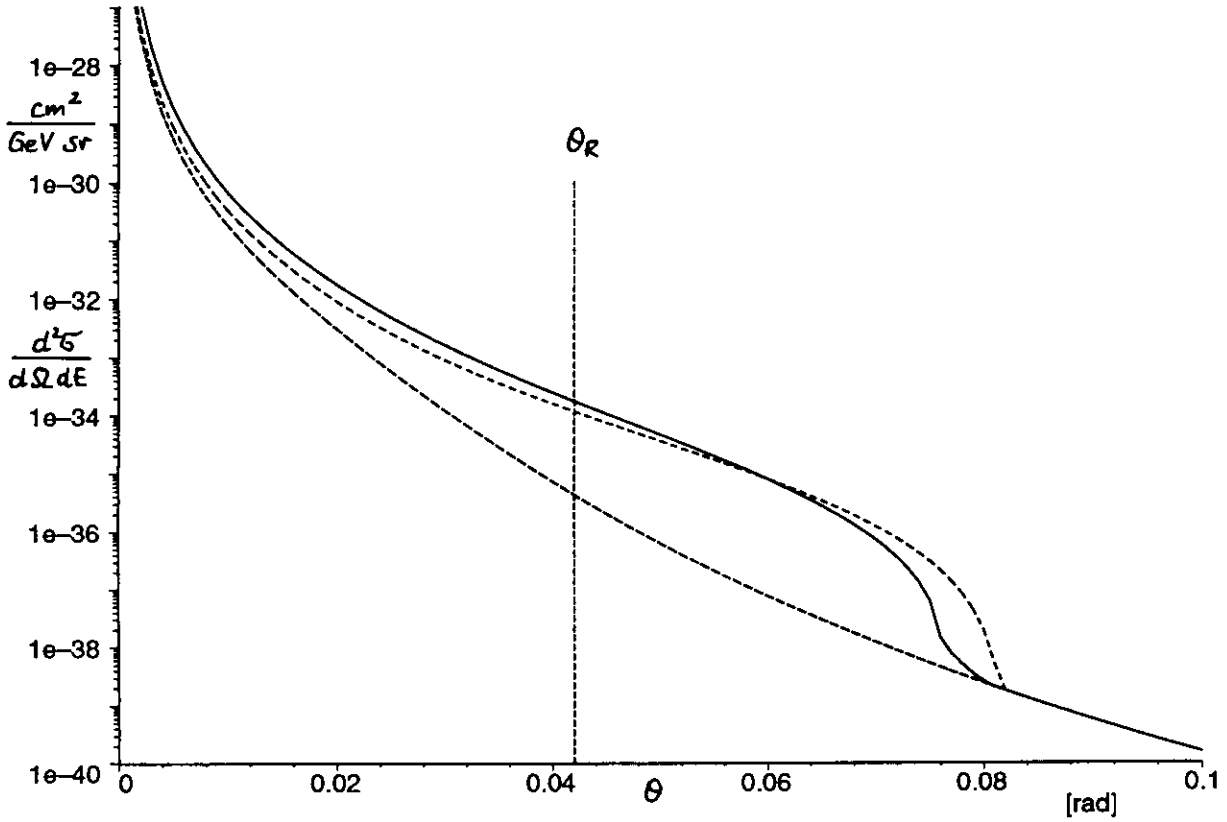
8

Figure 4: Muon production cross-sections for carbon at a photon energy of 200 GeV and a muon energy of 120 GeV. Solid curve: full cross-section (see equ.(14)). Lower dashed curve: coherent contribution. Upper dashed curve: simplified full cross-section for dose calculation (see eqs.(14),(15)).

this is shown in fig.4. Nevertheless, the use of a nucleon-based cross-section with form factor gives the generally correct behaviour in the variables k,E and θ and the substitution $m_N = m_p$ the right kinematics. In fig.4 one sees an overestimation due to the parametrization in equ.(15) at the kinematical limit and a slight underestimation for smaller angles being of no interest for us. These properties are valid in the whole of photon energies from 50 GeV to 250 GeV and all muon energies which was explicetly checked by the authors.

The parameters Z=1 and $d' = 3$ GeV^2 were chosen to get a conservative dose estimation. They were neither fitted nor optimized. For any other applications or energy ranges the parameter d' has to be looked at carefully.

9

4 Dose calculations

Muon doses at earth surface were calculated with the formalism outlined in section 2 and the cross-section recieved in section 3.

Fig.5 gives an example for a beam loss of $3.7 \cdot 10^{21}$ electrons of 250 GeV per year and constant 10 m layer of soil above the target. The doses from coherent and incoherent pair production processes were calculated separately. The dose in the region near the target is dominated by the incoherent processes whereas the dose far from the target mainly stems from the coherent one.
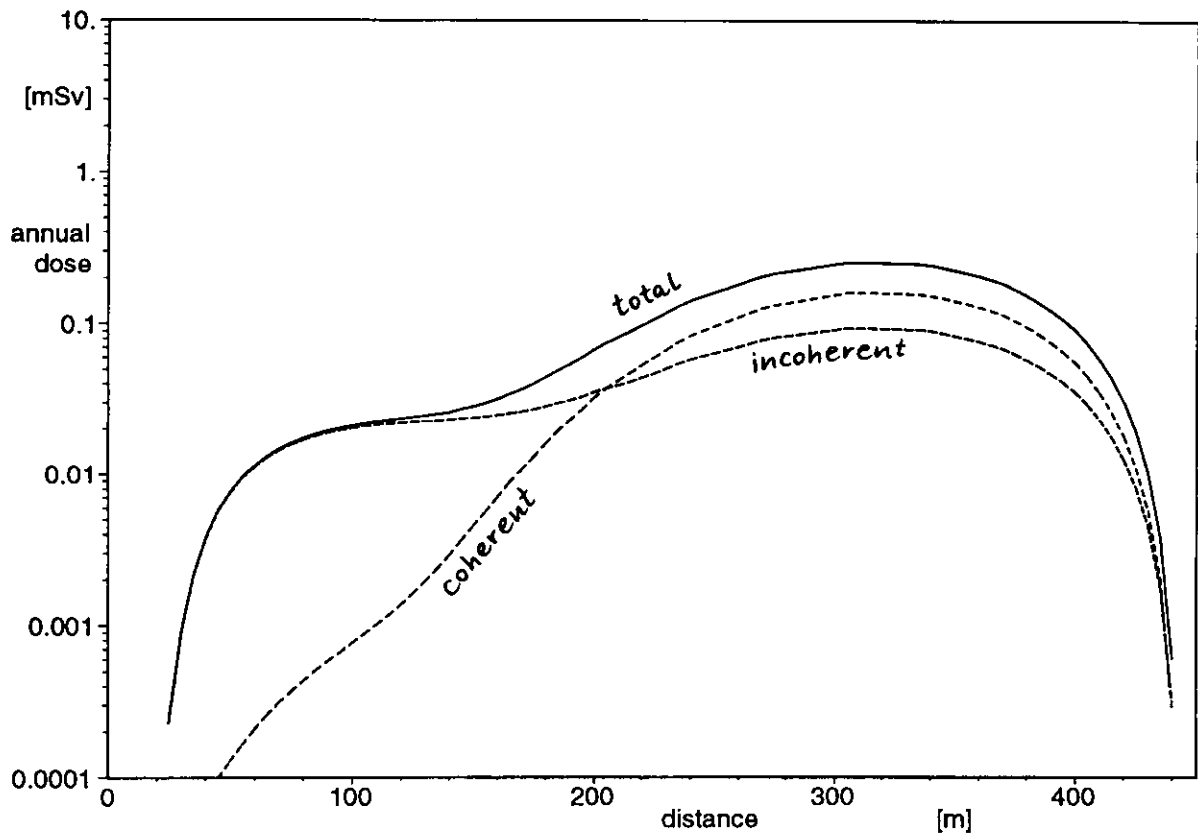

Figure 5: Annual doses as a function of distance from the target in beam direction at the earth surface. The soil layer is 10 m thick. Solid line: total dose, dashed lines: coherent and incoherent contributions.

The dose calculations for actual cases were performed with a primary electron energy of 250 GeV and for a run period of 5000 hours per year. The muon sources, beam losses and minimal soil layer thicknesses are listed in the table. The critical components are those of the positron linac. For details see our previous report [1].

10

Muon source	Beam loss	Soil layer downstream the target
Electron collimator	20 % of 8 MW	14 m
Positron collimator	20 % of 8 MW	10 m
Electron dump	8 MW	16 m
Positron dump	8 MW	12 m

In the fig.6 the annual dose profiles are plotted for the muon sources of the positron linac. For the maximum annual doses we get $50\,\mu$Sv produced by the positron collimator and $10\,\mu$Sv from the positron dump. Muon doses produced by the electron collimator and by the electron dump are less than $0.1\,\mu$Sv due to the thicker soil layers above.
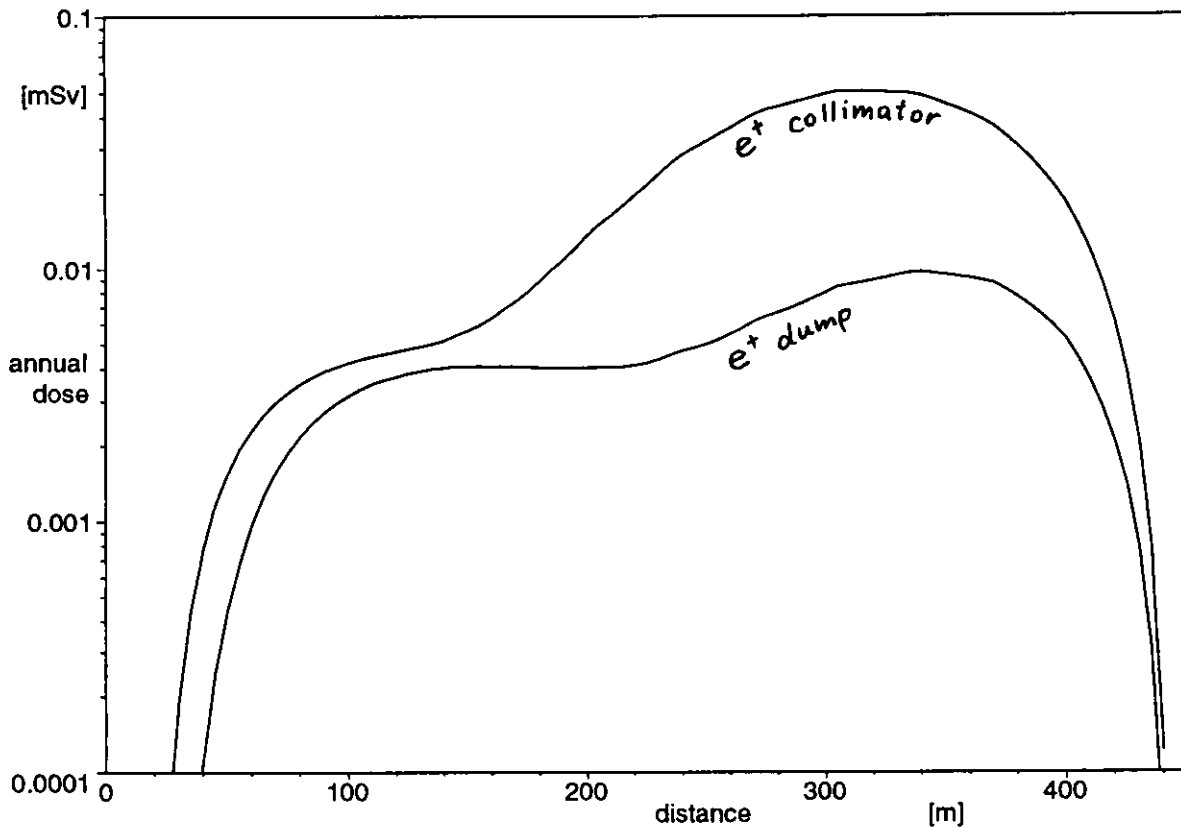

Figure 6: Annual doses as a function of distance from the target in beam direction at the earth surface. (Upper curve: positron collimator, lower curve: positron dump)

The muon field above the tunnel is roughly a corridor 450 m long and about 2 tunnel diameters wide starting directly above the target (collimator, dump) and following right along the direction of the primary beam.

In the case of an upgrade to 500 GeV beams with 16 MW each and with the targets at the same positions the corridor becomes 750 m long and the doses are doubled. They are still a factor of 10 below the natural background.

References

[1] A. Leuschner, K. Tesch: *Muon doses at earth surface above the Linear Collider.* Internal Report, DESY D3-89, Februar 1998

[2] W.R. Nelson: *The shielding of muons around high energy electron accelerators: theory and measurements.* Nucl.Instr.Meth. 66(1968)293

[3] W.R. Nelson, K.R. Kase: *Muon shielding around high energy electron accelerators.* Nucl.Instr.Meth. 120(1974)401

[4] Y.S. Tsai: *Pair production and bremsstrahlung of charged leptons.* Rev.Mod.Phys. 46(1974)815

[5] K.J. Kim, Y.S. Tsai: *Improved Weizsäcker-Williams Method and Its Application to Lepton and W-Boson Pair Production.* Phys.Rev. D8(1973)3109

[6] M. Chen, P. Zerwas: *Equivalent-particle approximation in electron and photon processes of higher-order QED.* Phys.Rev. D12(1975)187

[7] G. Chanfray et al.: *Quasi-elastic delta excitation in the charge response of the nucleus.* Nucl. Phys. A556(1993)439

[8] V.N. Baier, V.S. Fadin, V.H. Khoze: *Quasi-real electron method in high energy quantum electrodynamics.* Nucl. Phys. B65(1973)381

[9] R.M. Barnett et al.: *Review of Particle Properties.* Phys.Rev. D54(1996)1

[10] G. Baur, A. Leuschner: *To be published.* (1999)